Architecture of Metallic Nanoparticles by a Galvanic Redox Reaction

The quest for nanoscale architecture has demanded newer synthetic strategies for generating and manipulating nanoscopic metal crystals. This article reports the feasibility of a galvanic redox reaction as a novel synthesis strategy to architect metallic nanocrystals (NCs) with well-defined structures. Herein, we demonstrate galvanic redox reaction strategy to generate $Fe_{1-x}PtRu_x$ ternary metal NCs from FePt NCs and monometallic Pd NCs from Ag NCs. However, this methodology can easily be extended to generate other kinds of metallic NCs in solution. The unique application of X-ray absorption spectroscopy (XAS) in confirming the chemical transformation and getting structural insights during the architecture of metal NCs has also been demonstrated. Our method has opened a new route to easily and rapidly prepare a solid-solution type of metal NCs for potential catalytic applications.

Compared to conventional sequential reduction strategies, galvanic redox process has several advantages for the fabrication of core-shell type nanocrystals (NCs): (1) no additional reducing agent is needed and (2) spontaneous shell layer deposition occurs on top of the core particle surface. It suggests that the galvanic redox reaction of nanocrystals would be a quite useful method for the preparation of other new types of nanostructures. In case of Ag-Pd nanoparticles, the studies on Ag nanocrystals in the presence of Pd^{2+} ions in AOT reverse micelles have shown that the replacement reaction resulted in Pd NCs with a significant structure transformation. The driving force of this specific reaction of the nanocrystals was attributed to the differences of the reduction potentials between Ag and Pd.

The PtRu nanocrystals have been the subject of intense investigations because of their unique catalytic properties for fuel cell applications. The change in atomic distribution of PtRu NCs has great influence on their electrocatalytic activity. It is of great importance to generate a new type of metal NCs with improved catalytic performance to replace expensive Pt and Ru metals and to increase their atomic distribution for the commercial purpose. In this report, we selected FePt nanocrystals (NCs) and the Ru^{3+} ions as reactants to produce ternary metal NCs of $Fe_{1-x}PtRu_x$ using a galvanic redox reaction in a solution (Figure 1). The XAS results suggested that iron atoms of FePt lattices were oxidized to be Fe^{2+} and Fe^{3+} ions and were replaced by Ru atoms obtained from the reduction of Ru^{3+} ions

Beamlines

01C Extended X-ray Absorption Fine Structure

SP12B2 Protein X-ray Crystallography

17C Extended X-ray Absorption Fine Structure

Authors

D. Y. Wang and C. C. Chen
National Taiwan Normal University, Taipei, Taiwan

B. J. Hwang, C. H. Chen, L. S. Sarma, J. M. Chen, S. C. Shih and G. R. Wang
National Taiwan University of Science and Technology, Taipei, Taiwan

B. J. Hwang, J. F. Lee, M. T. Tang, H. S. Sheu, and D. G. Liu
National Synchrotron Radiation Research Center, Hsinchu, Taiwan

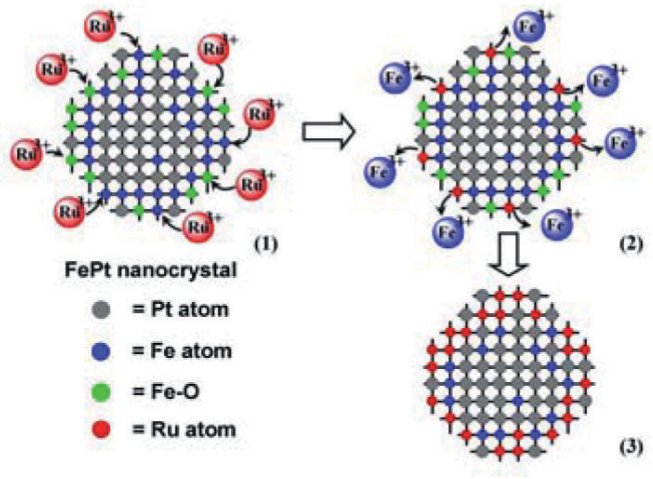

Fig. 1: Schematic illustration of chemical transformation from FePt to $Fe_{1-x}PtRu_x$ NCs. (1) Ru^{3+} ions and FePt NCs. (2) galvanic redox reaction between Ru^{3+} ions and Fe species. (3) production of ternary $Fe_{1-x}PtRu_x$ NCs.

in solution to form $Fe_{1-x}PtRu_x$ lattices.

The starting materials, FePt NCs, were synthesized by following the previous report with some modifications. High-resolution TEM images of resulting FePt NCs in Figure 2a have shown that the nanocrystals were crystalline with clear lattice structures. The nanocrystals were uniform and well-dispersed on the TEM grid with an average diameter of ~4 nm. The solution of FePt NCs was then allowed to react with the Ru^{3+} ions at 85˚C. The typical TEM image (Fig. 2b) of the resulting $Fe_{1-x}PtRu_x$ NCs revealed that there was no significant change on the averaged size and shape of $Fe_{1-x}PtRu_x$ NCs in comparison to those of original FePt NCs (Fig. 2a).

The Fe/Ru ratio of $Fe_{1-x}PtRu_x$ NCs formed under typical reaction time of 1 hour is calculated from XAS by measuring the edge jump is 0.27/0.73. The overall results suggested that metal ions, Ru^{3+}, were indeed reduced to be metal atoms of $Fe_{1-x}PtRu_x$ NCs and iron atoms of FePt NCs were oxidized and released as Fe^{2+} and Fe^{3+} in the solution.

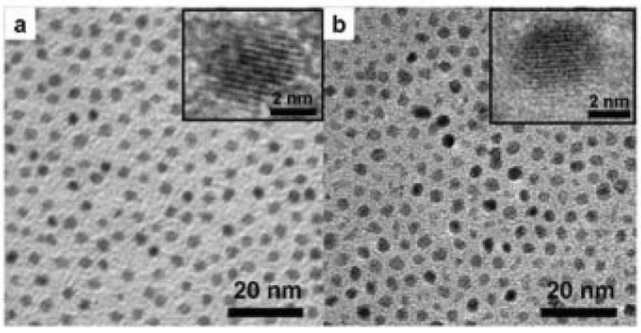

Fig. 2: High-resolution TEM images of (a) FePt and (b) $Fe_{1-x}PtRu_x$ NCs.

To further understand the redox reaction between the FePt NCs and the Ru^{3+} ions, synchrotron XAS was performed on the samples of FePt and $Fe_{1-x}PtRu_x$ NCs. The Fe K-edge XANES spectra of FePt powder and reference compounds (Fe foil, FeC_2O_4, and $FePO_4$) are shown in Figure 3a. The edge energy position of the FePt is found to be located between the Fe foil and FeC_2O_4 reference compounds, indicating that the iron element in FePt NCs is a mixture of Fe^0 and Fe^{2+}. Figure 3b shows that the white line features of FePt and $Fe_{1-x}PtRu_x$ samples are similar to that of Pt foil, implying that the oxidation state of Pt in the FePt and $Fe_{1-x}PtRu_x$ NCs retained to be Pt^0. The composition of iron in $Fe_{1-x}PtRu_x$ NCs is too low to get a good spectral resolution of EXAFS at Fe K-edge, indicating that a large number of the Fe atoms have been replaced by the Ru atoms. However, Ru elements can be observed at Ru K-edge for the $Fe_{1-x}PtRu_x$ sample.

The XANES feature of Ru K-edge for the $Fe_{1-x}PtRu_x$ NCs is close to that of the Ru reference as shown in Figure 3c, indicating that most of the Ru species have been reduced to Ru^0 state. It is suggested that the Fe atoms in the bimetallic NCs can react with Ru^{3+} via the replacement reaction. The electrons required for the reduction of Ru^{3+} ions are contributed from the oxidation of Fe^0 to Fe^{3+} or Fe^{2+} to Fe^{3+}.

The structural parameters extracted from the EXAFS spectra for the FePt and $Fe_{1-x}PtRu_x$ NCs were listed in Table 1, in which the fitting was on the basis of the fcc structure and the FeO crystal structure, respectively. The Fe K-edge EXAFS of the FePt NCs (not shown here) shows Fe-O peak between 1.3 and 2.0 Å. It is believed that the FeO species would be dispersed on the surface of the FePt NCs. The coordination number of N_{Pt-Fe} and N_{Pt-Pt} is found to be 1.7 and 6.8 for the FePt NCs and 0.4 and 6.8 for the $Fe_{1-x}PtRu_x$ NCs, respectively (Table 1). The decrease in N_{Pt-Fe} from 1.7 in the FePt sample to 0.4 in the $Fe_{1-x}PtRu_x$ sample, implied that most of the iron atoms are dissolved after $RuCl_3$ addition consistent with XANES observations. The total coordination number of metallic Fe atoms (5.6) is much smaller than that of metallic Pt atoms (8.5) in the case of FePt, indicating that the Pt atoms and Fe atoms are rich in the core region and in shell region, respectively, in the nanocrystals. For the structural model of the FePt NCs, the overall results suggest that most of the Pt atoms are preferentially located in the core region, the Fe atoms are preferentially located in the shell region, and small amount of the FeO

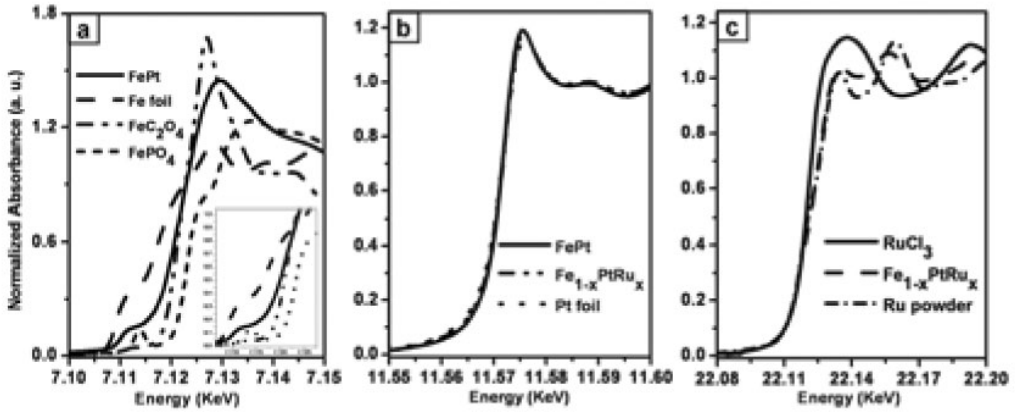

Fig. 3: Normalized XANES spectra near the (a) Fe K-edge, (b) Pt L_{III}-edge, and (c) Ru K-edge.

species are dispersed on the FePt NC's surface. For a P_{core}-R_{shell} nanocrystal model, if all the P atoms are occupied in the core region, the total coordination number of P core atoms should be 12 based on the fcc structure. However, the total coordination number of Pt atoms is 8.5 and 7.2 for the FePt and $Fe_{1-x}PtRu_x$ NCs, respectively, indicating that some of surface sites are occupied by Pt atoms in the shell regions for both samples.

The fitting result shows that the coordination numbers of Cl, Fe, and Ru around Ru are found to be 2.7, 1.2, and 3.3 respectively. The Cl coordination would be attributed to the residual $RuCl_3$ after the galvanic redox reaction. Both $N_{Pt\text{-}Ru}$ and $N_{Ru\text{-}Pt}$ cannot be extracted and only shows the Pt-Fe and Ru-Fe bonds, indicating a three-stacking region in the $Fe_{1-x}PtRu_x$ NCs (Ru-Fe/Fe/Fe-Pt). For the structural model of $Fe_{1-x}PtRu_x$ NCs, these observations indicate that most of the Pt atoms are preferentially located in the core region and the Ru atoms are located in the shell region with an intermediate iron-layer between the Pt and Ru atoms. In conclusion, our results have demonstrated a simple and rapid route for the syntheses of new catalysts based on metal alloy nanocrystals.

Tab. 1: Structural parameters derived from the Fe K-edge, Pt L_{III}-edge, and Ru K-edge XAS.

Sample	Edge	shell	N	R_j(Å)	σ^2(x10^{-3})(Å^2)	ΔE_0(eV)
FePt	Fe	Fe-O	3.2	1.899	5.0	-18.0
	K-edge	Fe-Pt	5.6	2.683	7.9	2.7
		Fe-Fe	3.8	3.190	0.0	13.7
	Pt	Pt-Fe	1.7	2.683	7.2	3.9
	L_{III}-edge	Pt-Pt	6.8	2.736	6.0	4.1
$Fe_{1-x}PtRu_x$	Pt	Pt-Fe	0.4	2.724	0.0	3.9
	L_{III}-edge	Pt-Pt	6.8	2.736	6.2	3.8
	Ru	Ru-Cl	2.7	2.347	0.0	17.3
	K-edge	Ru-Fe	1.2	2.573	8.0	12.2
		Ru-Ru	3.3	2.717	0.0	-13.6

N: coordination number, $\mathbf{R_j}$: bonding distance, σ^2: Debye-Waller factor, $\Delta\mathbf{E_0}$: Inner potential shift.

Experimental Stations

X-ray absorption spectroscopy station
X-ray powder diffraction station
Protein crystallography station

Publications

. B.-J. Hwang, C.-H. Chen, L. S. Sarma, J.-M. Chen, G.-R. Wang, M.-T. Tang, D.-G. Liu, and J.-F. Lee, *J. Phys. Chem.* B, **110**, 6475 (2006).
. C.-H. Chen, L. S. Sarma, G.-R. Wang, J.-M. Chen, S.-C. Shih, M.-T. Tang, D.-G. Liu, J.-F. Lee, and B.-J. Hwang, *J. Phys. Chem.* B, **110**, 10287 (2006).
. D.-Y. Wang, C.-H. Chen, H.-J. Yan, Y.-L. Lin, P.-Y. Huang, B.-J. Hwang, C.-C. Chen, *J. Am. Chem. Soc.*, **129**, 1538 (2007).
. L. S. Sarma, C.-H. Chen, S.-C. Yen, G.-R. Wang, S. M. S. Kumar, K.-L. Yu, D.-G. Liu, H.-S. Sheu, M.-T. Tang, J.-F. Lee, C. Bock, K. H. Chen, and B.-J. Hwang, *Langmuir*, DOI: **10.1021**/la0637418 (2007).
. B.-J. Hwang, L. S. Sarma, G.-R. Wang, C.-H. Chen, D.-G. Liu, H.-S. Sheu, and J.-F. Lee, *Chemistry - A European Journal* (**2007**). (in press)

Contact E-mail

bjh@mail.ntust.edu.tw